Contact Resonance Imaging with Vertical Nanowire Arrays

Michael Fahrbach, M. Sc.[a], Dr.-Ing Jiushuai Xu[a], Mgr. Petr Klapetek Ph.D.[b,c], Assoc. Prof. Mgr. Jan Martinek Ph.D.[b,d], Prof. Dr. Erwin Peiner[a]

[a] Technische Universität Braunschweig, Institute of Semiconductor Technology (IHT), Hans-Sommer-Straße 66 and Laboratory for Emerging Nanometrology (LENA), Langer Kamp 6a/b, 38106 Braunschweig, Germany

[b] Czech Metrology Institute, Okružní 31, 638 00 Brno, Czech Republic

[c] CEITEC BUT, Purkyňova 123, Brno 612 00, Czech Republic

[d] Brno University of Technology, Faculty of Civil Engineering, Žižkova 17, Czech Republic

Abstract

A setup for high-throughput measurement of dimensional and mechanical parameters of silicon microwire and resist nanowire arrays is used for combined topography and contact resonance imaging. It is based on customized long slender piezoresistive silicon microprobes designed for in-line measurements of industrial workpieces. In measurements with microwire and nanowire arrays we found sub-micrometer resolution on large areas (300×300 µm^2) at high speed up to 300 µm/s. Using a mass-spring model, characteristic features of contact-resonance imaging with slender microprobes were simulated.

1 Introduction

Contact resonance (CR) spectroscopy or force microscopy (CR-FM) is an operation mode of atomic force microscopes (AFM) for imaging the mechanical properties of samples with nanoscale lateral resolution [1, 2]. In Atomic Force Acoustic Microscopy (AFAM), CR modes of the cantilever are excited via the sample, which is mounted on an external transducer. From the spectral position and shape of the CR mode, the contact mechanics, i. e., contact stiffness and damping, are derived, which provide information on the sample's viscoelasticity. Alternatively, an actuator in the cantilever holder can be employed for CR excitation which is then known as Ultrasonic Atomic Force Microscopy (UAFM). In the case of macro-scale samples like industrial workpieces only UAFM is feasible. For tactile sensing of the elastic properties of arbitrary materials, a "forefinger-like" piezoelectric cantilever was reported, which, however, has a mm-tip radius, i. e., is not suitable for scanning or imaging with µm-lateral resolution [3]. This resolution can be achieved with piezoresis-tive silicon cantilevers with µm-tip radius, using which height and CR scans across an array of silicon wires of a height, diameter, and pitch of 4 µm, 1.2 µm, and 3.2 µm, respectively, were demonstrated [4].

Recently, semiconductor nanowires (NWs) were moved into the focus as basic building block of energy haversting and storage devices. Harvesting electrical energy from ambient sources, such as temperature, vibrations and radiation to charge batteries will enable self-powered nodes in IOT applications, eliminating the need for wired power supplies. Semiconductor NWs offer low thermal conductivity, large specific surface, 1D current path, etc. for efficient energy harvesting by thermoelectric, piezoelectric and photovoltaic generation [5, 6]. Additionally, NWs can accommodate stress by the volume expansion of high-capacity Si anodes by Li intercalation during charging of Li ion batteries [7]. Massive parallelisation of NWs, e.g. in vertical arrays (NWAs) on a common (silicon) substrate, enables to combine energy harvesting and storage devices with other microelectronic devices in monothic Si chip designs (including sensors, data processing, and wireless data transmission). Future large-scale manufacturing of NWAs with defined dimensions, i.e., diameter, length, pitch, order, roughness, viscoelasticity, etc., e. g., in an industrial semicondcutor facility will require suitable high-throughput metrological tools. Wang et al. [8] showed, that mechanical characterization of NWs using AFM-based methods including CR can reveal their unique properties with respect to the bulk. However, they only performed CR measurements with single NWs, which were attached horizontally to a carrier substrate instead of vertical NWs in an array. Investigations are lacking on CR imaging (CRI) with vertical NWAs, which can be expected to be a powerful tool for measuring both dimensional an viscoelastic properties of NWAs. In this work, we therefore describe CRI of NWAs in a new-developed setup, shown in Figure 1, using piezoresistive cantilever sensors, which were recently introduced for combined topography and mechanical properties imaging in a commercial AFM as well as for in-line measurements on paper-making rolls under industrial conditions [9, 10]. Imaging was performed using both point-by-point probing and line-by-line scanning combined with line-shape analysis (LSA) of CR peaks and automatic-gain control (AGC)/CR-frequency tracking based on real-time phase-lock-loop (PLL) control, respectively.

ISBN 978-3-8007-5835-7

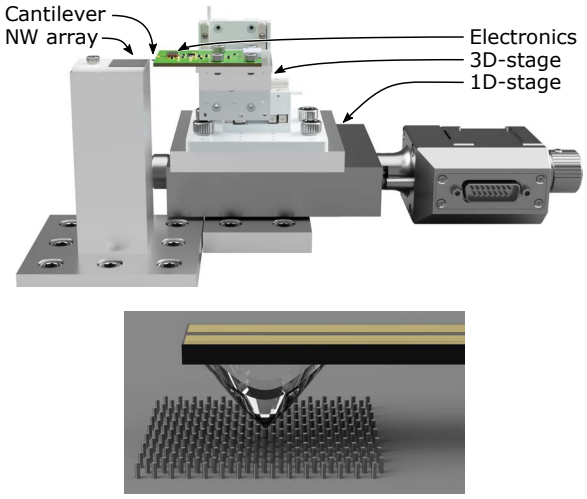

Figure 1 Render of the tactile-probing setup showing a cantilever with its tip in contact to a silicon micro wire array (MWA). **(Top)** Overview and **(bottom)** magnified view of the contact area. Electronics consist of amplifiers for the piezoresistive strain gauge and an interface for all relevant signals. 3D-piezo-stick-slip-stage for precision probe positioning and scanning (SmarAct SLS-3232-LC, range: 21 mm, max. speed: 20 mm/s, repeatability: 100 nm), and 1D-DC-motor-stage (PI M-126.PD1, range: 25 mm, max. speed: 15 mm/s, repeatability: 1 µm) for high-speed, long-distance scanning.

2 Experimental

Figure 1 shows in a schematic, as core component the probing stage of the new-developed CRI setup based on a piezoresistive tactile cantilever sensor (parameters see [9]), its carrier PCB and positioning and scanning stages, the cantilever with its tip in contact with an NWA (inset). A schematic of the measurement electronics is shown in Figure 2. The electronics include a signal generator with programmable amplitude, phase, frequency and offset, a piezo driver, a Lock-in amplifier, an ADC and a microcontroller. The microcontroller controls the amplitude and phase of the sensor real-time via the excitation amplitude and frequency in a digital AGC and PLL, respectively. The measured data is acquired and stored on a personal computer (PC, not shown here), which additionally controls the probing force (given by the DC contribution to the sensor's output voltage) by adjusting the z-position of the piezo stage with a time constant of approx. 25 ms. This time constant was selected to minimize the influence of impulses that are created during stick-slip cycles of the 3D-stage. It will be reduced in following studies.

Figure 3 shows in its left part a silicon micro wire array, with height, diameter, and pitch of 4 µm, 1.2 µm, and 4 µm, respectively, fabricated using ultraviolet based soft nanoimprint lithography (soft UV-NIL) and deep reactive ion etching at cryogenic temperature (cryo DRIE) [11]. With such MWAs, Young's moduli measured by nanoindentation and CR-FM were reported, which differ considerably from their bulk counterparts [11]. In addition, we investigated a mr-UVCur06 nanoimprint resist NWA, which

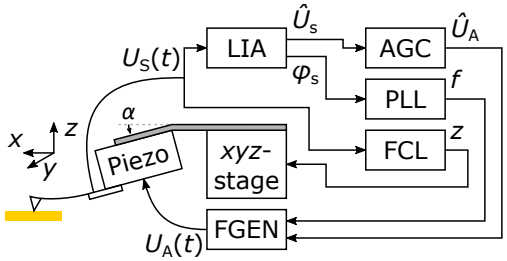

Figure 2 Schematic of the CRI setup. The sensor is mounted, via a piezoactuator, on an xyz-stage at the tilt angle α. It is actuated out-of-plane by the out-of-plane piezoactuator while its probing tip is in contact with the surface of a sample. The resulting mechanical vibration is converted into an electrical signal by a piezoresistive strain gauge, that is integrated into the cantilever. The output signal of the strain gauge $U_S(t) = \hat{U}_S \times \cos(2\pi ft + \varphi_S) + \overline{U}_S$ is connected to a Lock-in amplifier (LIA) to obtain the amplitude $\hat{U}_S$ and phase φ_S of the vibration, respectively. The amplitude is kept constant using an automatic gain control (AGC) that adjusts the actuation amplitude $\hat{U}_A$. The phase is kept constant using a phase-locked loop (PLL) that adjusts the actuation frequency f. The actuation signal $U_A(t) = \hat{U}_A \times \cos(2\pi ft)$ is generated using a direct digital synthesis (DDS) based frequency generator (FGEN) and supplied to the piezoactuator. Additionally, the DC-component of the output signal of the strain gauge $\overline{U}_S$, which is related to the static probing force, is kept constant using a force-control loop (FCL), which is implemented on an external PC, that adjusts the z-position of the xyz-stage.

is shown in the right part of this figure.

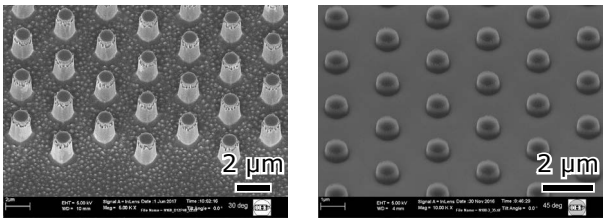

Figure 3 Scanning electron microscopy (SEM) photographs of **(left)** a (100)-silicon MWA of height, diameter, and pitch of 4 µm, 1.2 µm, and 4 µm, respectively and **(right)** a mr-UVCur06 resist NWA on silicon of height, diameter, and pitch of 0.5 µm, 0.8 µm, and 2.6 µm, respectively.

3 Results and discussion

Figure 4 shows the CR spectrum of the fundamental resonance mode of the piezoresistive cantilever probe measured with a (100)-silicon micro wire. By fitting a Fano-resonance line shape to the measured magnitude and phase (Fano LSA) [12], we obtain the resonance frequency f_0, quality factor Q and amplitude, which are related to the tip-to-wire contact stiffness and damping.

Point-by-point frequency-sweeps, with steps of 1 Hz over

ISBN 978-3-8007-5835-7

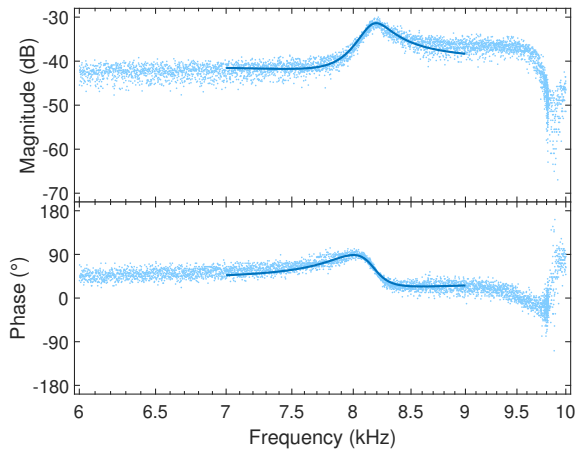

Figure 4 Magnitude and phase vs. frequency around the fundamental resonance mode; measured on a Silicon micro wire. Line-shape analysis (LSA, solid line) was done by fitting a Fano-resonance line shape (Fano LSA) [12] yielding $f_0 = 8.169$ kHz and $Q = 29.5$.

a range of 5 kHz around f_0, are performed and followed by spectral analysis based on Fano LSA [12]. Typical height and CR images of the MWA are shown in Figure 5. The total time per point of approx. 1.85 s is given by tip 0.7 s approach, 0.95 s dwell/frequency sweep and 0.2 s retraction. This compares reasonably with the speed of mechanical mapping mode in AFM [13]. Measurements were performed at a maximum sample rate of 6 kS/s, a bandwidth of 1 kHz and a resolution of 14 Bit.

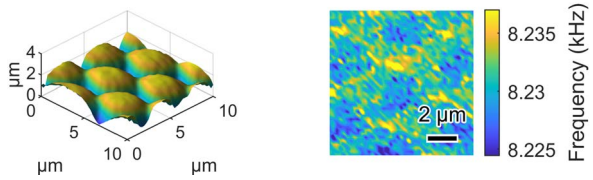

Figure 5 **(Left)** Topography and **(right)** contact-resonance image of the silicon MWA measured point-by-point at 10 µN. The cantilever was tilted by 15°.

The MWA with its 6-fold symmetry of NW arrangement is visible in both images. Although the obtained pitch of the MWA corresponds to the designed value and the value measured using SEM, the wire height does not. Theoretically, as shown in Figure 6, the probing tip with a cone angle of approx. 40° should be able to reach approx. 4.7 µm beneath the top surface of the wires. The lower measured maximum wire height of approx. 2 µm can be assigned to tip wear [14].

Furthermore, we performed line-scanning measurements with the same sample using the digital PLL. Here, the cantilever was tilted by 15° and one-way scanned parallel to its axis. For each scan line, the acceleration of the stage was limited to 1 mm/s^2. The maximum speed was selected between 1 µm/s and 500 µm/s. Figure 7 clearly shows the MWA with its 6-fold symmetry of NW arrangement, however, with a blurred contrast in the scanned topography image but a clearer frequency contrast in the CRI.

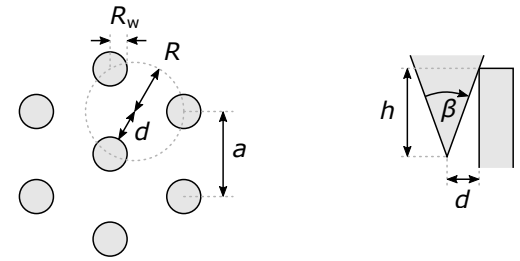

Figure 6 **(Left)** Top view of a regular hexagonal micro- or nanowire array showing the wire pitch a, the wire radius R_w, the radius of the circumcircle of the equilateral triangles $R = a/\sqrt{3}$, and the maximum lateral distance between the apex of the probing and the sidewall of a wire $d = R - R_w$. **(Right)** Side view of a conical probing tip with cone angle β next to a wire. The maximum probing depth is given by $h = d/\tan(\beta/2)$.

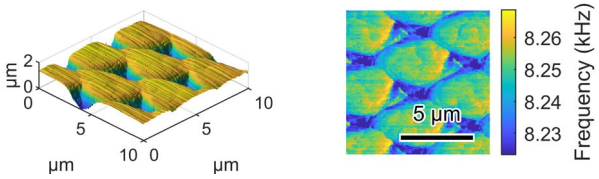

Figure 7 **(Left)** Topography and **(right)** contact-resonance image of the silicon MWA measured by line-by-line scanning at 1 µm/s and 10 µN. The cantilever was tilted by 15°.

As the next step we increased the image area to 300 × 300 µm^2, which was scanned at a speeds of 5 µm/s and 500 µm/s. The latter is above the range of high-speed AFM scanning [15]. The measured topography and CR images of the silicon MWA are shown in Figures 8 and 9.

Enlarged sections of both show the expected six-fold symmetry. However, drift is visible, which can be attributed to temperature variations during the image acquisition time of approx. 10.5 h. During this measurement the tip exhibited further wear resulting in blurring of the following topography and contact-resonance images. This can also be seen in the following measurement at 500 µm/s in Figure 9, which was acquired within 40 min. The hexagonal symmetry is still visible in the detail enlargements but cannot be resolved properly at higher scanning speed, i. e., in the image sections towards the center of the line scans.

In Figure 10 we show point-by-point measurements with the resist NWA of Figure 3. The hexagonal arrangement of the NWs is clearly visible in both images. The height, diameter and pitch values from the topography image agree well with values approximated from the SEM image in Figure 3. In the CRI, a more pronounced contrast occurs, which we assign to the elasticity differences between resist and silicon. In this case, due to the much lower height of the NWs, the tip could reach the silicon surface between the wires. Between two wires, where the tip was in contact with a wire only via its sidewall and not with the bottom silicon surface, we observe the lowest frequencies.

ISBN 978-3-8007-5835-7

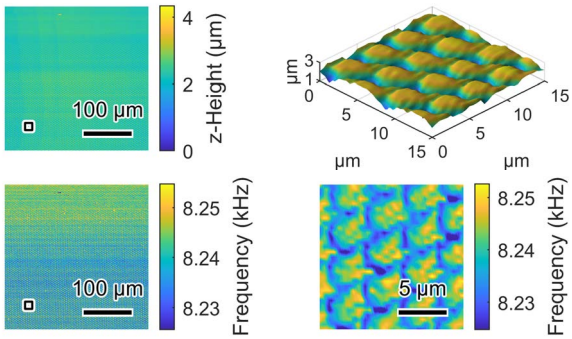

Figure 8 **(Top)** Large-area (300 × 300 µm^2) topography and **(bottom)** contact-resonance images of the silicon MWA measured using line-by-line scanning at 5 µm/s and 10 µN. The cantilever was tilted by 15°. The figures on the right show corresponding magnified views of the highlighted areas to the left. Here the sample rate was reduced to 1 kS/s to reduce the file size of the measured data.

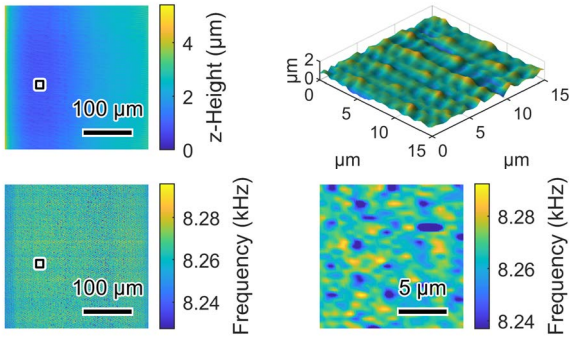

Figure 9 **(Top)** Large-area (300 × 300 µm^2) topography and **(bottom)** contact-resonance images of the silicon MWA measured using line scanning at 500 µm/s and 10 µN. The cantilever was tilted by 15°. The figures on the right show corresponding magnified views of the highlighted areas to the left. The MWA topography was only resolved properly at speeds below approx. 300 µm/s.

To better understand the phenomena related to CRI on complex samples like nanopillars on substrate, we have setup a simple mass-spring model capable of simulating some aspects of the imaging process. The mass-spring model is based on creating a network of point masses interconnected by springs, as described in [16]. The masses movement is calculated by integrating the Newton equations. As the model was originally designed for static calculations, for purposes of this work it was validated by comparison to Finite Element Modeling (FEM) while performing modal analysis of cantilevers of various geometries, showing that the mass spring model errors for dynamic calculations are up to 10 %, similarly to the static calculations.

The model was setup using geometrical primitives as shown in Figure 11. Model discretisation was 1 µm and masses and springs between them were assigned to have the mechanical properties of silicon. The auxiliary area

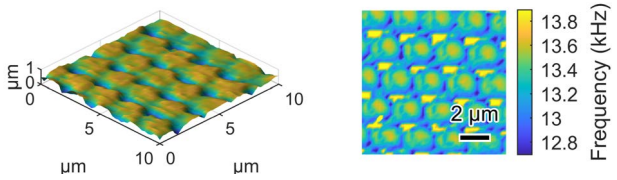

Figure 10 **(Left)** Topography and **(right)** second-mode contact-resonance image of the resist NWA measured point-by-point at 10 µN. The cantilever was aligned parallel to the sample surface.

forming the upper part of the probe was filled with about 7 times denser material having 8000 times lower elastic modulus. This creates a virtual spring array mimicking the properties of the cantilever, effectively reducing the base resonance frequency of the whole system by few orders of magnitude. Even with this arrangement, we were able to mimic only relatively stiff probes (with resonance frequencies in range of hundreds of kHz, i.e. ten times higher than the microprobes used for the experiments). Nevertheless, we believe that the phenomena that can be handled by this model are relevant also for the softer probes. The calculation was performed by applying a pulse mechanical excitation to the probe and storing the displacement of mass points in the sample from their steady state position. These data were processed by a Fourier transform to obtain a vibrational spectrum of the system.

By placing the probe on different locations on the sample and running the calculation we can obtain map frequencies that would be observed in the contact resonance experiment, as shown in Figure 11, where an area surrounding one nanopillar was mapped. We can see that the effect of edge predomintantly leads to decrease of the resonant frequency which could be caused both by presence of less material in the contact area and added possibility of the nanowire to move in the lateral direction. However, also some points of higher frequencies can be seen and in total the edge leads to a very high variance of the resonance frequencies. In contrast to this, the mean resonance frequency on the flat nanowire top is only about 0.2 % lower than on the silicon substrate. This is below the numerical method accuracy, but still can illustrate that the impact of topography is much larger than the impact of local mechanical properties.

All these effects are also illustrated on details of the spectra around the fundamental frequencies when the probe is at different locations on the sample. From this graph we can also see that the frequency resolution is quite poor and the model could be refined both in the frequency domain (running much longer calculations) and in the spatial domain (using finer discretisation), which will be subject of our next study.

4 Conclusion

A setup was described for combined topography and contact-resonance imaging based on customized long slender piezoresistive silicon microprobes for in-line measure-

ISBN 978-3-8007-5835-7

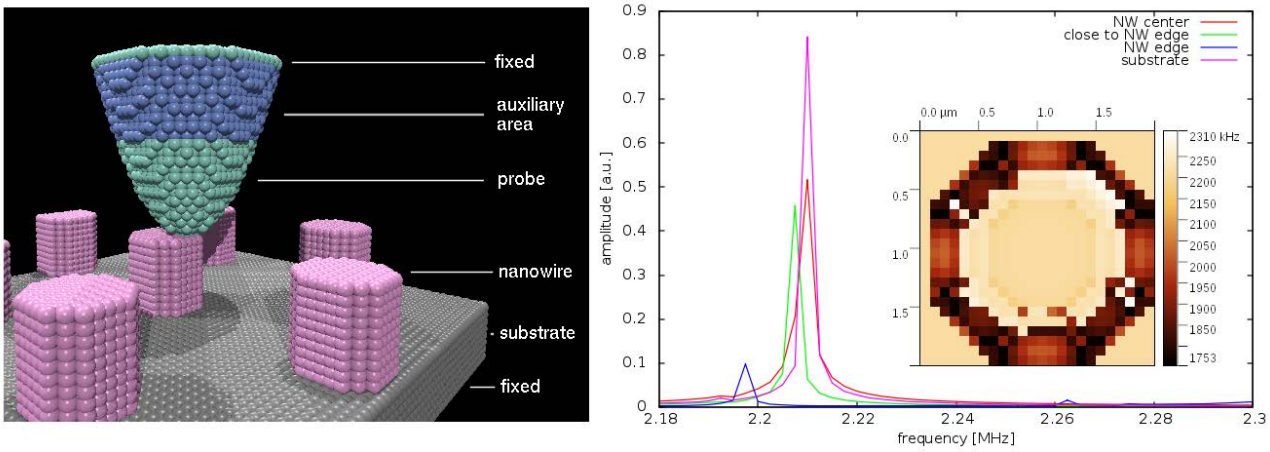

Figure 11 **(Left)** Schematic of the numerical model showing its key functional elements, **(right)** graph showing vibrational spectrum of the system for different positions of the probe, inset shows map of base resonance frequencies when scanning around one of the nanowires, obtained by the Fourier analysis and fitting the positions of the maxima.

ments of industrial workpieces. Point-by-point frequency-sweep measurements combined with line-shape analysis of contact resonance peaks were shown as well as line-by-line scanning under automatic-gain control and phase-lock-loop-based contact-resonance frequency tracking with silicon microwire and nanoimprint-resist nanowire arrays. Real-time imaging was demonstrated showing sub-micrometer resolution at high speeds up to 300 µm/s on large areas (300×300 µm^2). Characteristic aspects of the contact-resonance imaging process were simulated using a mass-spring model.

5 Acknowledgements

This study is performed in the NanoWires project (19ENG05), which has received funding from the EMPIR programme co-financed by the Participating States and from the European Union's Horizon 2020 research and innovation programme.

Literature

[1] Rabe, U. "Atomic Force Acoustic Microscopy". In: *Applied Scanning Probe Methods II*. Ed. by Bhushan, B. and Fuchs, H. NanoScience and Technology. Springer Berlin Heidelberg, 2006, pp. 37–90. DOI: 10.1007/3-540-27453-7_2.

[2] Hurley, D. C. and Killgore, J. P. "Dynamic Contact AFM Methods for Nanomechanical Properties". In: *Scanning Probe Microscopy in Industrial Applications: Nanomechanical Characterization*. John Wiley & Sons, Inc, 2013, pp. 115–149. DOI: 10.1002/9781118723111.ch5.

[3] Fu, J. and Li, F. "A forefinger-like tactile sensor for elasticity sensing based on piezoelectric cantilevers". In: *Sensors and Actuators A: Physical* 234 (2015), pp. 351–358. DOI: 10.1016/j.sna.2015.09.031.

[4] Bertke, M., Fahrbach, M., Hamdana, G., Xu, J., Wasisto, H. S., and Peiner, E. "Contact resonance spectroscopy for on-the-machine manufactory monitoring". In: *Sensors and Actuators A: Physical* 279 (2018): *EUROSENSORS 2017*, pp. 501–508. DOI: 10.1016/j.sna.2018.06.012.

[5] Mokkapati, S. and Jagadish, C., eds. *Nanowires for energy applications*. Semiconductors and Semimetals 98. Cambridge, MA: Academic Press, 2018.

[6] Goktas, N. I., Wilson, P., Ghukasyan, A., Wagner, D., McNamee, S., and LaPierre, R. R. "Nanowires for energy: A review". In: *Applied Physics Reviews* 5.4 (2018), p. 041305. DOI: 10.1063/1.5054842.

[7] Refino, A. D., Yulianto, N., Syamsu, I., Nugroho, A. P., Hawari, N. H., Syring, A., Kartini, E., Iskandar, F., Voss, T., Sumboja, A., Peiner, E., and Wasisto, H. S. "Versatilely tuned vertical silicon nanowire arrays by cryogenic reactive ion etching as a lithium-ion battery anode". In: *Scientific Reports* 11.1 (2021), p. 19779. DOI: 10.1038/s41598-021-99173-4.

[8] Wang, S., Shan, Z., and Huang, H. "The Mechanical Properties of Nanowires". In: *Advanced Science* 4.4 (2017), p. 1600332. DOI: 10.1002/advs.201600332.

[9] Fahrbach, M., Friedrich, S., Behle, H., Xu, M., Cappella, B., Brand, U., and Peiner, E. "Customized piezoresistive microprobes for combined imaging of topography and mechanical properties". In: *Measurement: Sensors* 15 (2021), p. 100042. DOI: 10.1016/j.measen.2021.100042.

[10] Teir, L., Lindstedt, T., Widmaier, T., Hemming, B., Brand, U., Fahrbach, M., Peiner, E., and Lassila, A. "In-Line Measurement of the Surface Texture of Rolls Using Long Slender Piezoresistive Microprobes". In: *Sensors* 21.17 (2021): *Cantilever Sensors for Industrial Applications*. Ed. by Tiribilli, B., p. 5955. DOI: 10.3390/s21175955.

[11] Hamdana, G., Puranto, P., Langfahl-Klabes, J., Li, Z., Pohlenz, F., Xu, M., Granz, T., Bertke, M., Wasisto, H. S., Brand, U., and Peiner, E. “Nanoindentation of crystalline silicon pillars fabricated by soft UV nanoimprint lithography and cryogenic deep reactive ion etching”. In: *Sensors and Actuators A: Physical* 283 (2018): *EUROSENSORS 2017*, pp. 65–78. DOI: 10.1016/j.sna.2018.09.035.

[12] Fahrbach, M., Nyang’au, W. O., Domanov, O., Schwalb, C. H., Xu, M., Li, Z., Kuhlmann, C., Brand, U., and Peiner, E. “Damped silicon microprobes for high-speed roughness measurements”. In: *Proceedings*. MikroSystemTechnik Kongress 2021 (Forum am Schlosspark, Ludwigsburg, Germany, Nov. 8–10, 2021). Berlin, Offenbach: VDE VERLAG GMBH, 2021. Chap. B4 Robuste & zuverlässige Mikrosysteme (1), pp. 118–121. URL: https://ieeexplore.ieee.org/document/9698292.

[13] Alunda, B. O. and Lee, Y. J. “Review: Cantilever-Based Sensors for High Speed Atomic Force Microscopy”. In: *Sensors* 20.17 (2020): *Cantilever-Based Sensors*, p. 4784. DOI: 10.3390/s20174784.

[14] Xu, M., Zhou, Z., Ahbe, T., Peiner, E., and Brand, U. “Using a Tip Characterizer to Investigate Microprobe Silicon Tip Geometry Variation in Roughness Measurements”. In: *Sensors* 22.3 (2022): *Cantilever Sensors for Industrial Applications*. Ed. by Tiribilli, B., p. 1298. DOI: 10.3390/s22031298.

[15] Glover, C. C., Killgore, J. P., and Tung, R. C. “Scanning speed phenomenon in contact-resonance atomic force microscopy”. In: *Beilstein Journal of Nanotechnology* 9 (2018), pp. 945–952. DOI: 10.3762/bjnano.9.87.

[16] Klapetek, P., Campbell, A. C., and Buršíková, V. “Fast mechanical model for probe–sample elastic deformation estimation in scanning probe microscopy”. In: *Ultramicroscopy* 201 (2019), pp. 18–27. DOI: 10.1016/j.ultramic.2019.03.010.